



Numerical Investigation of Thermal-Hydraulic Performance of Printed Circuit Heat Exchanger with Different Fin Shape Inserts

Ali M. Aljelawy* , Amer M. Aldabbagh, Falah F. Hatem

Mechanical Engineering Dept., University of Technology-Iraq, Alsina'a street, 10066 Baghdad, Iraq.

*Corresponding author Email: [Ali M. Aljelawy_engaljelawy@gmail.com](mailto:Ali.M.Aljelawy_engaljelawy@gmail.com)

HIGHLIGHTS

- Numerical thermal and hydraulic analysis for a novel channel for mini channels printed circuit heat exchanger was done.
- Fins inserts of two different shapes have employed the diamond and biconvex shape fins
- The influence of two geometrical parameters was studied: the longitudinal and transverse pitch lengths.
- The results show a good enhancement in heat transfer indicated by the Nusselt number, but a fall in hydraulic performance indicated by the friction factor
- The overall performance factor criteria were employed to make the comparison with the straight rectangular channel depending on the same power input
- The new channels show a very good enhancement depending on the criteria

ARTICLE INFO

Handling editor: Jalal M. Jalil

Keywords:

Printed circuit heat exchanger; mini channel fluid flow; heat transfer; Nusselt number; friction factor.

ABSTRACT

The printed circuit heat exchanger is one of the most recent important heat exchangers, especially in the nuclear power plant and aerospace applications, due to its very compact geometry and small print foot. This paper presents a 3D numerical investigation of the thermo-hydraulic performance of PCHE with a new non-uniform channel design configuration. The new channel design consists of two different fins and shape inserts: the diamond and biconvex shapes. The influence of two design parameters on the heat exchanger performance was studied and optimized, the longitudinal and transverse pitch length (Pl) and (Pt). Air with constant properties as the working fluid with constant heat flux at the walls envelope. The Reynolds number varied from 200 to 2000. Different Pitch lengths were used (Pl=20, 30, 40, and 50) mm and (Pt=3, 4, and 5) mm. Three performance parameters were studied the Nusselt number, friction factor, and the overall performance evaluation factor. Results show that the thermal performance enhanced with decreasing the pitch lengths, and it was shown that this enhancement was found only at high Reynolds numbers above 1400. The higher enhancement factor was with NACA 0020 airfoil fins at pt=3 mm and pl=20mm of $\eta=2.75$ at Re=2000, while the worst performance was obtained with biconvex fins. The main reason behind the enhancement is the disruption of the boundary layer and the good mixing induced in the fluid flow.

1. Introduction

The printed circuit heat exchanger (PCHE), also called HEATRIC after the developer of this kind of heat exchanger, is a high integrity high compact plate type, heat exchanger. It has a unique design. It consists of many plates that are photo-chemically etched or pressed to form the flow passages configuration. Then the plates are stacked together and diffusion bonded (solid state joining) to form the block of the heat exchanger. The flow passages formed as semicircular sections because of the isotropic etching process with different configurations. PCHE is characterized by its high coefficient of heat transfer due to the high surface area to volume ratio and high-pressure drop due to the small diameter. It can withstand the high pressure of about 600 bar with large temperatures ranging from cryogenic to 700°C [1]. Fluid flow inside PCHE can be parallel flow, counter flow, cross flow, or a combination of these. PCHEs are extremely strong and compact and have a rich history of use in the refining industries, hydrocarbon processing, petrochemicals, and power generation due to their high effectiveness in energy recovery, energy storage, and solar thermal energy [1]. The thermal performance in PCHEs is mainly enhanced passively by introducing a complex flow channel. On the other hand, optimization must be done due to an expected increase in pressure drop. Previous studies on PCHEs focused on their thermal-hydraulic performance characteristics to increase the heat transfer rate with pressure drop as low as possible. Both experimental and numerical studies have been conducted at this point

of the research study. The heat transfer and pressure drop of straight flow channels PCHE were investigated numerically by Aneesh et al. [2], where the working fluid used were Helium. The influence of thermo-physical properties, operating conditions, and three design parameters were studied. The results showed that the single bank model (one hot and one cold plate alternatively) possesses better thermal-hydraulic performance than the double bank configuration (two hot plates and one cold plate alternatively). The same was noticed for aligned as compared with a staggered arrangement of cold and hot channels. Both pressures drop, and heat transfer increase with dimple inserts and increases with more dimples inserted. The effect of operating pressure on $s\text{CO}_2$ working fluid performance in PCHE with straight channels was investigated by Chu et al. [3]. The tests were performed with ($s\text{CO}_2$ -water) as the working fluids. The findings indicate that the heat transfer capability of water is lower than that of $s\text{CO}_2$ at the same mass flow rates. The pressure drop is the same for both water and $s\text{CO}_2$ below $m=300$ kg/min, while after that value, a difference will appear due to the decrease in CO_2 outlet temperature which in turns will increase the viscosity of CO_2 . Lee and Kim [4] conducted a numerical study to optimize the zigzag flow channels in PCHE of the double-faced type model. The non-dimensional pressure drop and the effectiveness of zigzag channels were chosen as the optimization's two reliable factors and three non-dimensional variables, namely the ratios of the wave height, wavelength, and fillet radius to the channels' hydraulic diameter were chosen as design parameters. The double face channel has higher effectiveness than the single face channel but has an identical friction factor. Then they studied the effect of adding a slim plate between the cold and hot channel regions [5]. Furthermore, the impact of increasing the overlap between the two channels on the thermal efficacy of a standard PCHE is investigated in order to determine the benefit of ascending the overlap between channel areas. The Nusselt number, thermal effectiveness, Colburn j-factor, and net exergy gain of the novel design are analyzed and compared to a reference, which is a typical PCHE design. The suggested design's thermal performance is higher than the compared design's.

Taylor et al. [6] investigated the thermal-hydraulic performance of PCHE numerically. The effect of two design parameters, namely the ellipse aspect ratio and channel angle of the zigzag flow channel pattern, were studied. The results show that the best effectiveness of PCHE was obtained at a channel angle of 110° . And the effectiveness increases with the increasing aspect ratio of the cold channel. In comparison, the friction factor increases with increasing the aspect ratio. Baek et al. [7] investigated the thermal-hydraulic performance of PCHE experimentally for use in the cryogenic temperature region, with Helium as the working fluid at cryogenic temperatures. The study also focused on the effect of axial conduction on thermal performance. They showed that axial conduction has a major influence in lowering the thermal performance of PCHE in a cryogenic environment, and its effect increases with increasing temperature due to increased thermal conductivity. Baik et al. [8] performed numerical and experimental investigation on the design and operation issues of PCHE as the pre-cooler in the supercritical CO_2 ($s\text{CO}_2$) power cycle. Moreover, a one-dimensional MATLAB code was developed for the design of PCHE.

The test conditions were for a temperature of $(26\text{--}43)^\circ\text{C}$ and pressure of $(7.3\text{--}8.6)$ MPa. PCHE of zigzag channel shape was used. CFD simulation was done to investigate the channel corner shape. The water side is laminar, while the CO_2 side is turbulent. The results show that a channel with a sharp corner showed a 40–65% larger pressure drop than a round corner due to reverse flow. And that reverse flow increases the thermal resistance and decreases the heat transfer rate. Moreover, the effect of vertical and horizontal arrangement of PCHE was studied by Kim and No [9] experimentally and numerically. Experiments were carried out in the laminar region. On the cold side, the numerical results for the vertical operation have excellent agreement with the actual data. However, those for the horizontal operation deviated substantially because of the non-uniform flow distribution of water in the horizontal arrangement. Therefore, researchers recommended the vertical arrangement for stable operation. Nusselt number correlation is suggested in terms of Prandtl number and Reynolds number. In contrast, the friction factor correlation in the PCHE was established using the Reynolds number and a correction factor, taking into account considerable temperature differences between the surface and bulk mean. Kim et al. [10] performed CFD analyses to evaluate heat transfer and pressure drop performance of wavy PCHE for the $s\text{CO}_2$ power cycle application for $\text{Re}=2000\text{--}58000$. By comparing CFD findings to experimental correlations, a novel CFD-aided correlation including the Reynolds number range 2000–58,000 for Nusselt number and friction factor is presented to help in the design of PCHEs for the supercritical CO_2 Brayton cycle application.

The channel cross-section shape has a major influence on thermal performance, so a comparative study has been made by Kim [11] using various channel cross-sectional shapes and channel configurations of a zigzag PCHE using 3-D Reynolds Averaged Navier Stokes (RANS). To measure the thermo-hydraulic performance of PCHE, effectiveness, the average Nusselt number, friction factor, and Colburn j-factor are employed. The impacts of four channel cross sections (semicircular, trapezoidal, circular, and rectangular) on thermal-hydraulic performance are investigated. The rectangular channel provides the greatest thermal performance but the worst hydraulic performance, while the circular channel provides the worse thermal performance. In cold channels, it is discovered that the friction factor and Colburn j-factor are inversely related to the Reynolds number. Still, the effectiveness and global Nusselt number are proportional to the Reynolds number. Lee and Kim [12] perform a numerical study to optimize Arc-shaped ribs in the zigzag cooling channels of PCHE to improve heat transfer and reduce the pressure drop based on three-dimensional RANS analysis and a multi-objective genetic algorithm with surrogate modeling. With the use of two geometric design factors (the ratios of the depth and pitch of the ribs to the channel hydraulic diameter).

In comparison to the reference design without ribs, the optimum designs exhibit significant enhancement in thermal performance and pressure drop. Effectiveness increased by 62.7 percent, and the friction factor was down 51.5 percent. Fernández and Sedano [13] presented a numerical study to investigate the performance of PCHE working with $s\text{CO}_2$ /eutectic lead-lithium in counter-current flow configuration. PCHE plates are made with fins of the airfoil shape. The airfoil forms and fins arrangement were optimized for pressure drop and heat transfer. The findings indicate that the smallest $\Delta p/Q$ ratio occurs at the maximum distance between airfoils. Cui et al. [14] investigated numerically the thermo-hydraulic performance of PCHE employing two novel air-foil fins based on NACA 0020 using $s\text{CO}_2$ as the working fluid.

The findings reveal that one of the two fins offers superior comprehensive performance than that of NACA 0020, which delivers lower pressure drop and greater j factor than NACA 0020 owing to the thinner boundary layer. The fins staggered arrangement enhances the heat transfer by decreasing the boundary layer effect. Ngo et al. [15] perform a 3D simulation to investigate the thermo-hydraulic performance of a new PCHE with an S-shaped fin configuration in a hot water supplier in which the cold water stream of 7°C is heated to 90°C using heat-exchange with sCO_2 of 118°C and 11.5 MPa temperature and pressure respectively. At fin angle of 52 and various fin sizes and hydraulic diameters for cold and hot channels. The better heat transfer performance obtains with a smaller hydraulic diameter. But the water channel's diameter must be sufficient to avoid obstruction caused by scale deposition from city water at temperatures more than 60 degrees Celsius. The new PCHE with S-shaped fins consumes 3.3 times less space than the previous hot water supply and results in a 37 percent reduction in CO_2 pressure drop and a tenfold reduction in water pressure drop. Aljelawy et al. [16] performed a numerical investigation of PCHE thermal-hydraulic performance using periodic diamond (converging-diverging) channels. Three geometrical parameters were studied: the pitch length of periodic section, length ratio of converging-diverging section and the angle of opening with Helium as the working fluid. Pitch length of ($1.59, 3.18, 6.36,$ and 12.73) mm, and angle of opening of ($0, 4.5, 6, 7.5, 9, 10.5$ and 12) and length ratio of ($0.2, 0.25$ and 0.333) were used for Reynolds number range of (200 - 2000). Results show that the thermal performance enhanced with decreasing the pitch length and with increasing C-D angle and it was shown that this enhancement was found only at high Reynolds number above 1400 . The best performance obtained at $p=3.18, \alpha=6$ and $\beta=0.25$ based on the overall evaluation performance.

The main aim of the present study is to find a new channel configuration that gives high thermal performance with less pressure drop. So, computational fluid dynamics (CFD) models were used to analyze the thermal-hydraulic performance of PCHE with different fin inserts: the biconvex, diamond, and NACA0020 airfoil fin shapes. In addition, two design factors were evaluated and optimized for heat exchanger performance, longitudinal and transverse pitch length (P_l) and (P_t) for laminar flow.

2. Numerical work

2.1 Computational Models

It is well known that there are two methods used to enhance heat transfer; the active method, which requires an external power addition, such as vibration, and the passive method. The latter is not required any external power addition such as extended surfaces disturbance and swirl generators (twisted tape, twisted tube, etc.).

In the present work, channels with fins insert are used to disturb the flow with three different shapes the diamond, the biconvex, and the NACA0020 airfoil shape. The three fins with dimensions are shown in Figure 1. In addition, two design parameters were studied: the longitudinal pitch length (P_l) and the transverse pitch length (P_t).

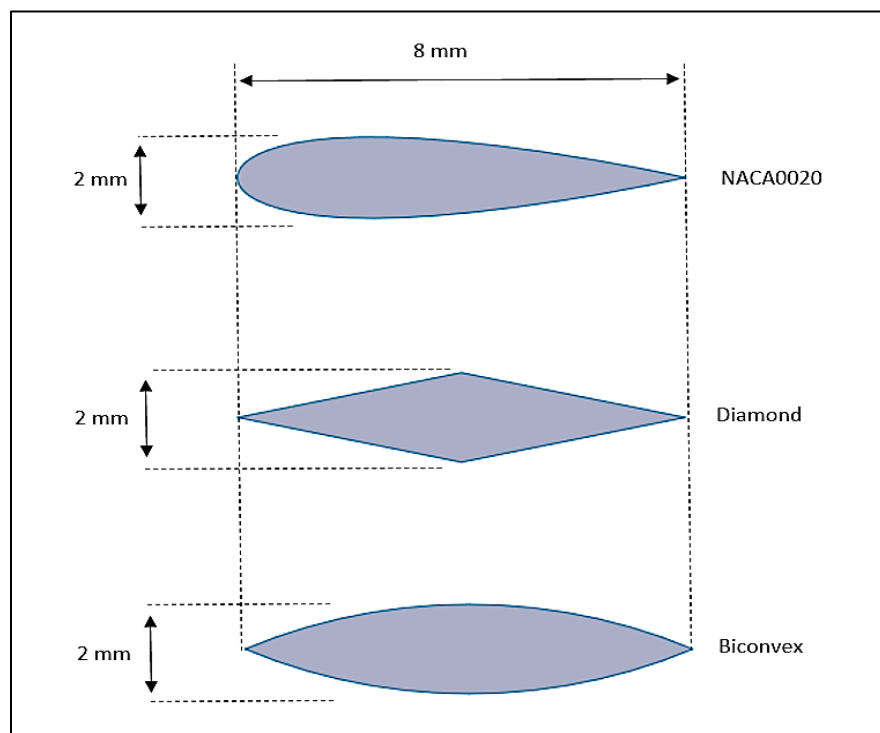


Figure 1: Biconvex, diamond, and NACA0020 shape fins

2.2 Mathematical Model

2.2.1 Assumptions

Mathematically, the problem was handled by taking the following assumptions:

- 1-Assuming that the flow is steady-state.
- 2-Three-dimensional flow.
- 3-Continuum.
- 4-Constant fluid thermo-physical properties.
- 5-Incompressible and Newtonian fluid flow.
- 6-Neglecting gravitational forces in all directions.
- 7-Neglecting viscous dissipation and heat generation for energy equation.

2.2.2 Governing equations

The commercial software ANSYS FLUENT 18.0 is employed for solving the governing equations, which include Continuity, momentum and energy equation and are listed as follows[17].

continuity

$$\frac{\partial u}{\partial x} + \frac{\partial v}{\partial y} + \frac{\partial w}{\partial z} = 0 \quad (1)$$

Momentum x- component:

$$\rho \left(u \frac{\partial u}{\partial x} + v \frac{\partial u}{\partial y} + w \frac{\partial u}{\partial z} \right) = -\frac{\partial p}{\partial x} + \mu \left(\frac{\partial^2 u}{\partial x^2} + \frac{\partial^2 u}{\partial y^2} + \frac{\partial^2 u}{\partial z^2} \right) \quad (2)$$

Momentum y - component:

$$\rho \left(u \frac{\partial v}{\partial x} + v \frac{\partial v}{\partial y} + w \frac{\partial v}{\partial z} \right) = -\frac{\partial p}{\partial y} + \mu \left(\frac{\partial^2 v}{\partial x^2} + \frac{\partial^2 v}{\partial y^2} + \frac{\partial^2 v}{\partial z^2} \right) \quad (3)$$

Momentum z - component:

$$\rho \left(u \frac{\partial w}{\partial x} + v \frac{\partial w}{\partial y} + w \frac{\partial w}{\partial z} \right) = -\frac{\partial p}{\partial z} + \mu \left(\frac{\partial^2 w}{\partial x^2} + \frac{\partial^2 w}{\partial y^2} + \frac{\partial^2 w}{\partial z^2} \right) \quad (4)$$

Energy equation

$$\rho C_p \left(u \frac{\partial T}{\partial x} + v \frac{\partial T}{\partial y} + w \frac{\partial T}{\partial z} \right) = k \left(\frac{\partial^2 T}{\partial x^2} + \frac{\partial^2 T}{\partial y^2} + \frac{\partial^2 T}{\partial z^2} \right) \quad (5)$$

2.2.3 Boundary conditions

To solve the governing equations, we need boundary conditions, so the three-dimensional x,y, and z boundary conditions in the non-dimensional form are:

First of all, the non-dimensional parameters are described as follows:

$$Z=z/L, \quad Y=y/H, \quad X=x/W$$

$$U=u/u_{in}, \quad V=v/u_{in}, \quad W=w/u_{in}$$

Where : L: length of the channel, H: height of the channel, W: width of the channel,

So, for momentum boundary conditions

$$\text{At } Y=0 \quad U=V=W=0 \quad \text{no-slip condition}$$

$$\text{At } X=0 \text{ and } X=1 \quad \partial U/\partial X = 0, \quad \partial V/\partial X = 0 \text{ and } V=0 \quad \text{symmetry}$$

$$\text{At } Y=0.5 \quad \partial U/\partial Y = 0, \quad \partial V/\partial Y = 0 \text{ and } W=0 \quad \text{symmetry}$$

$$\text{At } Z=0 \quad U=V=0, \text{ and } W=1 \quad \text{inlet velocity}$$

$$\text{At } Z=1 \quad p_{abs}=p_{static} + p_{operating}, \quad p_{static}=0 \quad U,V \text{ and } W \text{ are extrapolated [18]}$$

While, for thermal boundary conditions

$$\text{At } Y=0 \quad q=-k\partial T/\partial Y \quad \text{wall heat flux}$$

$$\text{At } Y=0.5 \quad \partial T/\partial Y=0 \quad \text{symmetry}$$

$$\text{At } X=0 \text{ and } X=1 \quad \partial T/\partial X=0 \quad \text{symmetry}$$

$$\text{At } Z=0 \quad T=T_i \quad \text{inlet temperature}$$

$$\text{At } Z=1 \quad p_{static}=0, \quad \text{temperatures are extrapolated}$$

2.3 Numerical Method

A 3-D numerical simulation was carried out on the physical domain of a rectangular channel with inserted fins through the flow with a staggered distribution. The rectangular channel is 500 mm in length. The fins are 8mm long, 2mm wide and a height of the flow channel depth of 1mm. To reduce the computational cost, the asymmetric section of the channel with constant wall heat flux will be simulated with constant air properties, which is the working fluid. The physical domain is cleared in Figure 2 and Figure 3.

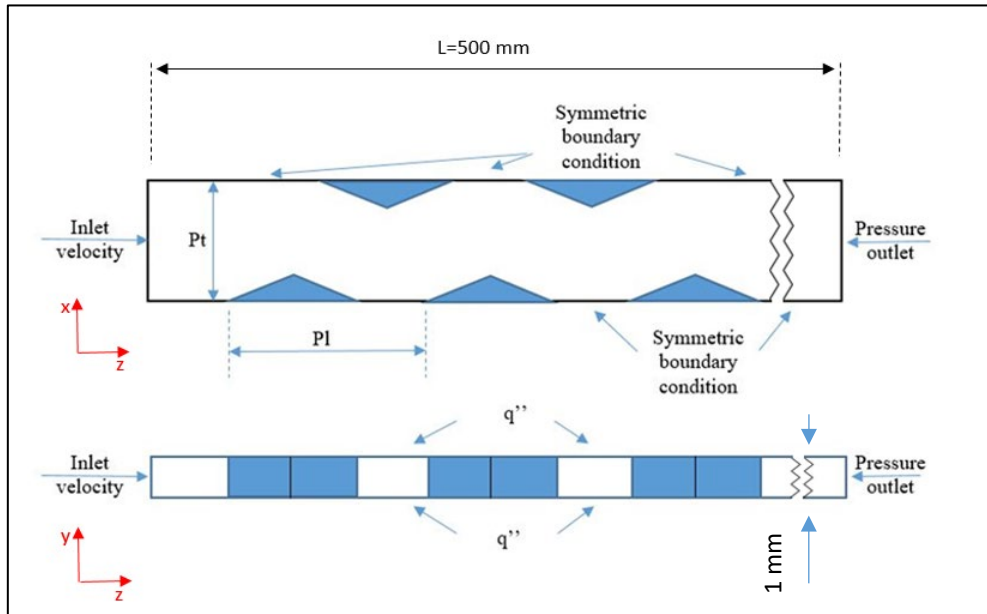


Figure 2: Top and side view of the physical geometry with boundary conditions

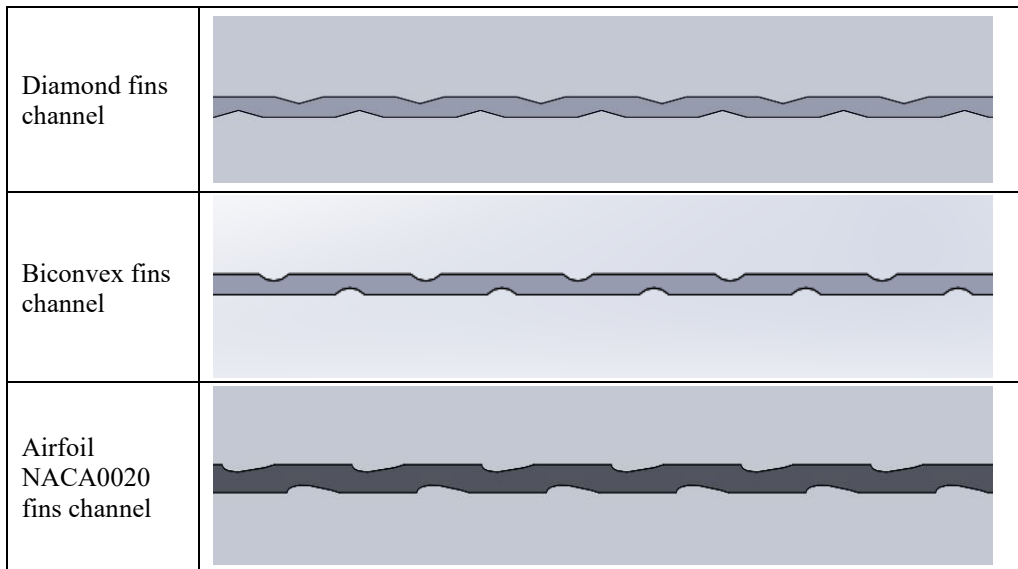


Figure 3: Top view of the physical geometry of the three fined channels

The segregated solver is used for solving the governing equations with double precision for higher accuracy. For convergence issues, the residual is set at 10^{-4} for Continuity and 10^{-6} for momentum and energy, and the quantities of interest are monitored. A structured grid of hexahedron cells is used with finer mesh near the wall with 3 prism layers to catch the boundary layer and reduce the mesh size, as shown in Figure 4. An independent grid study was performed for the maximum Reynold number of 2000 to obtain the optimum mesh size, as shown in Table 1.

To ensure the validity of the numerical work, a comparison was made with the experimental data of zigzag channel PCHE presented by Chen et al. [19], as shown in Figure 5, Figure 6, and Figure 7. Also, a reduced scale model was used of a single channel with constant wall heat flux with temperature-dependent properties of Helium as the working fluid. It was shown a good agreement with the experimental data published. However, the results show a little deviation, and this is not. The main reason for that deviation is the assumption of constant heat flux at the walls. At the same time, in the experiments of Chen et al. [19], the channels are subjected to the practical heat flux, which is neither a constant heat flux nor a constant wall temperature.

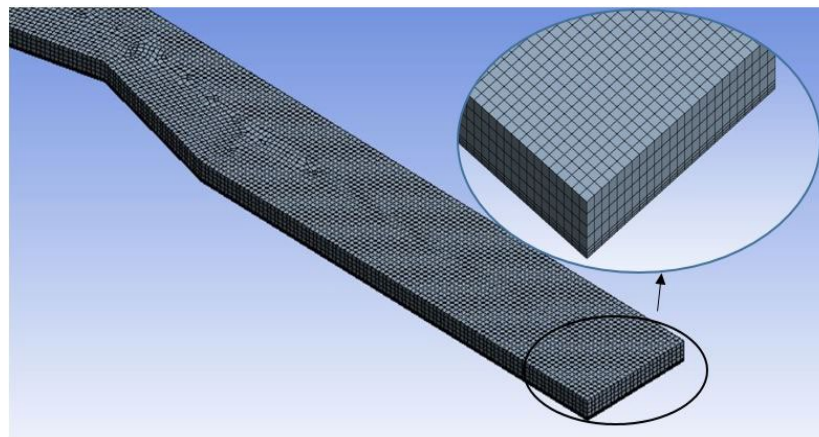


Figure 4: Mesh of PCHE channel analysis model

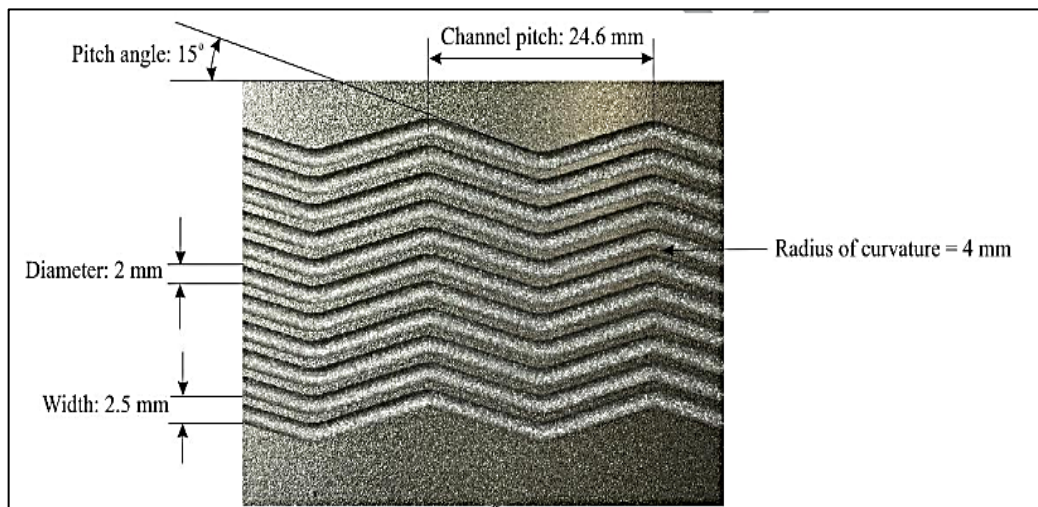


Figure 5: Zigzag channel from Chen et al [19]

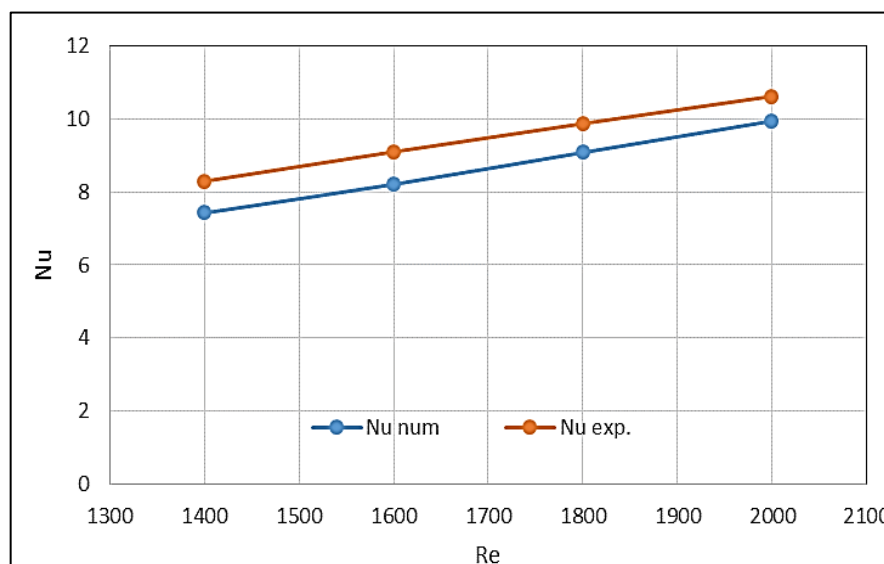


Figure 6: Comparison of numerical Nusselt number with experimental results of the zigzag channel from Chen et al. [19]

Table 1: Mesh independent test results

Cell count	Nu	%	f	%
915200	7.800621	---	0.015205	----
1806580	8.203682	5%	0.015593	3%
2779760	8.319968	1%	0.015729	1%
3984020	8.338743	1%	0.015852	1%

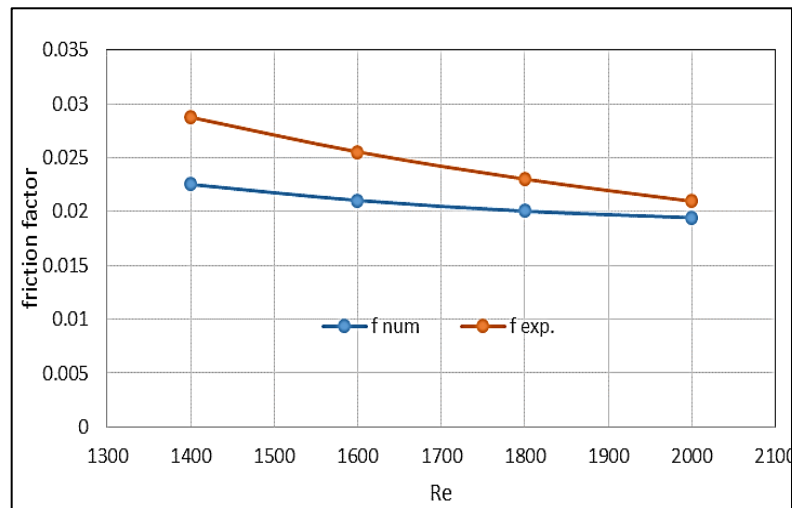


Figure 7: Numerical friction factor in comparison with experimental results of the zigzag channel from Chen et al. [19]

2.4 Data Reduction

The Nusselt number, friction factor, and the overall performance evaluation factor (η) are calculated from fluent data as follows:

$$Nu = \frac{hd_h}{k_f} \quad (6)$$

$$h = \frac{q''}{T_{\text{bulk}} - T_{\text{wall}}} \quad (7)$$

$$f_{\text{Fanning}} = \frac{1}{4} \Delta P \frac{Dh}{l} \frac{2}{\rho v^2} \quad (8)$$

$$\eta = \frac{(Nu/Nu_s)}{(f/f_s)^{1/3}} \quad (9)$$

Where q'' is the average heat flux, T_{wall} is the area average wall temperature and, T_{bulk} is the average helium bulk temperature, which is the mass-weighted average temperature. Nu_s represent the Nusselt number and friction factor for the smooth rectangular channel, d_h is the hydraulic diameter, which is the equivalent diameter along the channel. Also, it can be calculated as [20];

$$d_h = \frac{4A}{P} \quad (10)$$

3. Results and discussion

There are three main parameters of interest, Nusselt Number (Nu), friction factor (f), and the overall performance evaluation factor (η).

3.1 Nusselt Number

It turns out from the results that the Nusselt number increases with the Reynolds number increment for all cases. Figure 8 shows the effect of transverse pitch length (pt) on Nusselt number for the channel with diamond fins at pl=30 mm with different Reynolds numbers. It can be remarked that the Nusselt number exhibits two different behaviors: The Nusselt number increases with pt increment at a low Reynolds number. While, at high Reynolds number, Nusselt number decreases with pt increment. The increase of Nusselt number for pt=3 mm was (77%-154.7%) compared with the straight channel for Re= (200-2000), while for pt=5 mm was (95%-127.7%).

That enhancement in thermal performance is due to the disruption of the boundary layer at the fins region and the good mixing of fluid flow employing the core flow in the heat transfer process. The reason behind that inversion in behavior at smaller pitch lengths and high Reynolds number is the separation of the flow after the fins. In contrast, the separation occurs more early at the smaller pitch lengths. It leads to a greater stagnant flow area which will increase the thermal resistance by shadowing the heat transfer area as it clears in velocity contour in Figure 17.

Figure 9 shows the effect of longitudinal pitch length (pl) on Nusselt number for channels with diamond fins at pt=3mm with different Reynolds numbers. The longitudinal pitch length effect is similar to that of the transverse pitch effect. Whereas Nusselt number increases with pl increment at low Reynolds number, it decreases with pl increment at high Reynolds number. The percentage increment of Nusselt number for pl=20 mm of (65.4%-163%), while for pl=50 mm of (86.3%-124%) as compared with straight channel for Re= (200-2000).

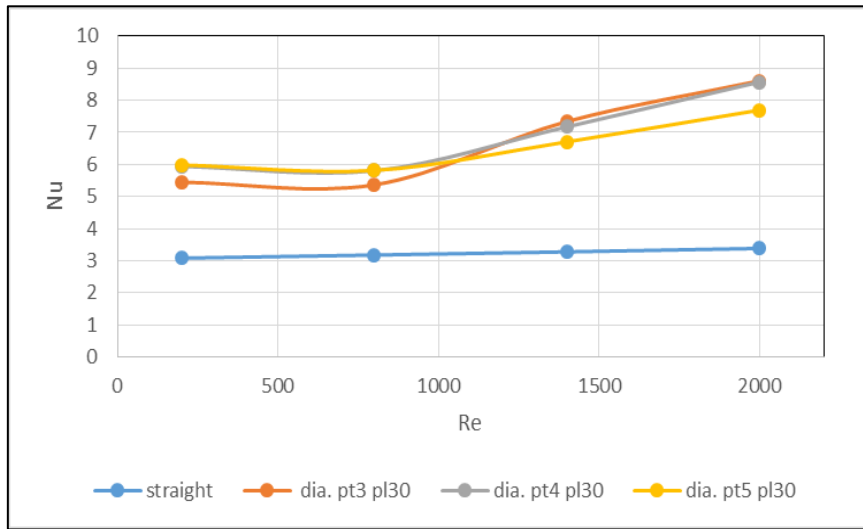


Figure 8: Effect of transverse pitch length on Nusselt number for diamond fins channel at pl=30 mm

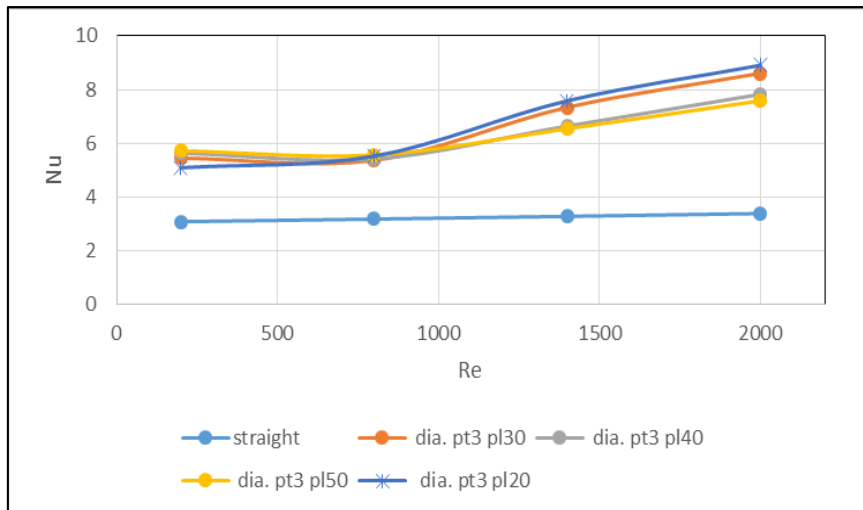


Figure 9: Effect of longitudinal pitch length on Nusselt number for diamond fins channel at pt=3 mm

Figures 10 and 11 show the effect of longitudinal pitch length (pl) on Nusselt number for a channel with biconvex and NACA0020 airfoil fins, respectively, at pt=3mm with different Reynolds numbers. It can be seen that the first behavior for the Nusselt number mentioned above is diminished for biconvex and airfoil fins, or it is confined at only the lowest Reynolds value. While for higher Reynolds value, Nusselt number decreases with pl increment. The increment of Nusselt number for p=20 mm was (1.64-2.58), while for p=30 mm was (1.82-2.62) times the straight channel for Re= (200-2000)

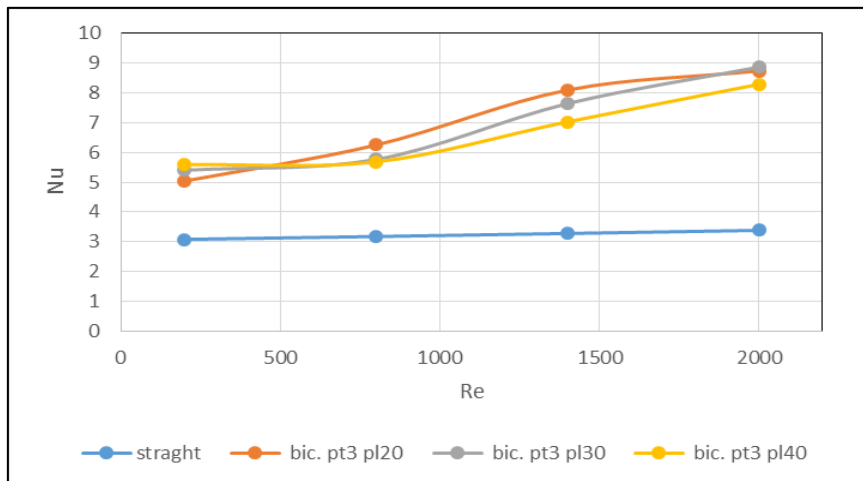


Figure 10: Effect of longitudinal pitch length on Nusselt number for biconvex fins channel at pt=3 mm

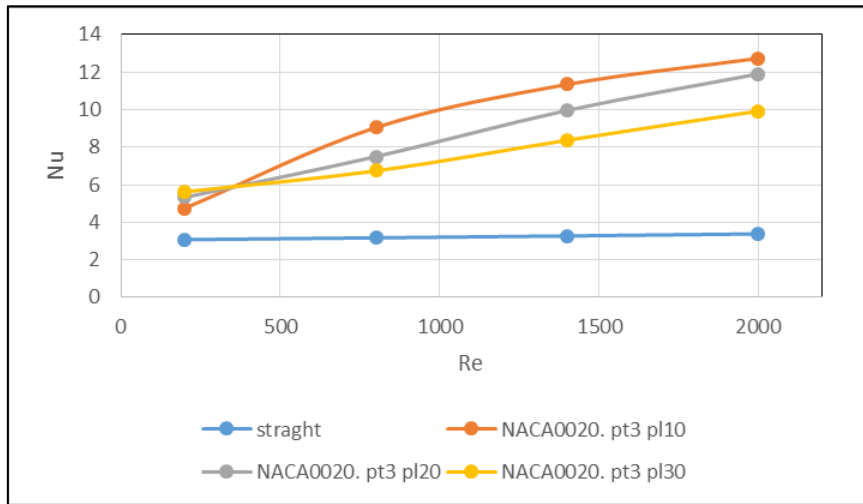


Figure 11: Effect of longitudinal pitch length on Nusselt number for NACA0020 airfoil fins channel at pt=3 mm

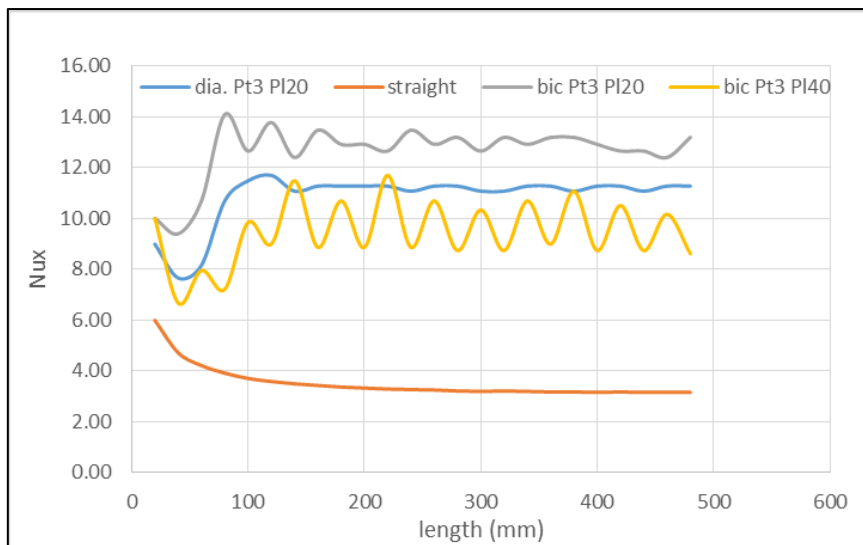


Figure 12: Local heat transfer coefficient along the channel for Re=2000

The local Nusselt number may indicate the thermal enhancement through the channel length, as shown in Figure 12. It shows that the Nusselt number decreases at the entrance length and as in a straight, smooth channel but suddenly increases for all cases and begins to fluctuate at almost fixed values. The Nusselt number sample points of p=20mm have been taken at the leading edge of the fins. This is why the Nu has almost a constant value. While, for p=40 mm, the samples were taken alternating once on the fins edge and once between the fins. Consequently, the trend is fluctuating.

3.2 Friction Factor

Friction factor as a representative pressure loss coefficient was used to evaluate the hydraulic performance. Figures 13 and 14 show the effect of transverse pitch length (pt) and longitudinal pitch length (pl) on friction factor for channels with diamond fins with different Reynolds numbers. It can be remarked that friction factor increases with pt decrement at the same pl. Whereas an increase of friction factor of (9%-105%) for pt=3mm compared with the straight channel. The longitudinal pitch length effect is similar to that of the transverse pitch effect, whereas the friction factor increases with pl decrement at the same pt. The rising rate of friction factor at pl=20 mm was (15%-124%) compared with a straight channel for Re= (200-2000). the decrease in pitch lengths increases flow distortion, as well as the area behind the fin where the separation induces. All of this increases the pressure drop. Moreover, it is common sense that friction increases with obstacles inserted in the flow field due to the drag force induced and also to the narrowing in the cross-section area or flow area

Figures 15 and 16 show the effect of longitudinal pitch length (pl) on friction factor for the channel with biconvex and NACA0020 airfoil fins, respectively, at pt=3mm with different Reynolds numbers. Also, it was found that friction factor increases with the decrease in pt for biconvex and airfoil fins channels. The rising rate in friction factor for the case of biconvex with pl=20 was about (15%-115%) compared with the straight channel for Re= (200-2000).

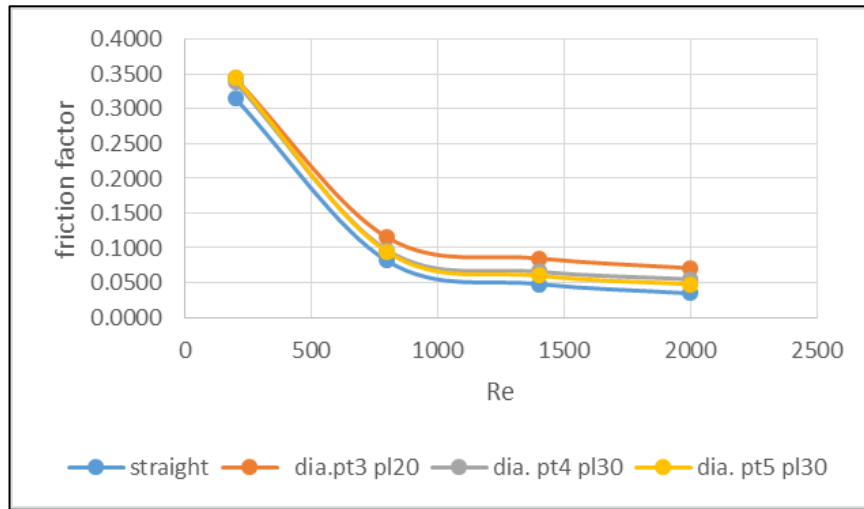


Figure 13: Friction factor versus Reynolds number for different transverse pitch lengths for diamond fins inserts

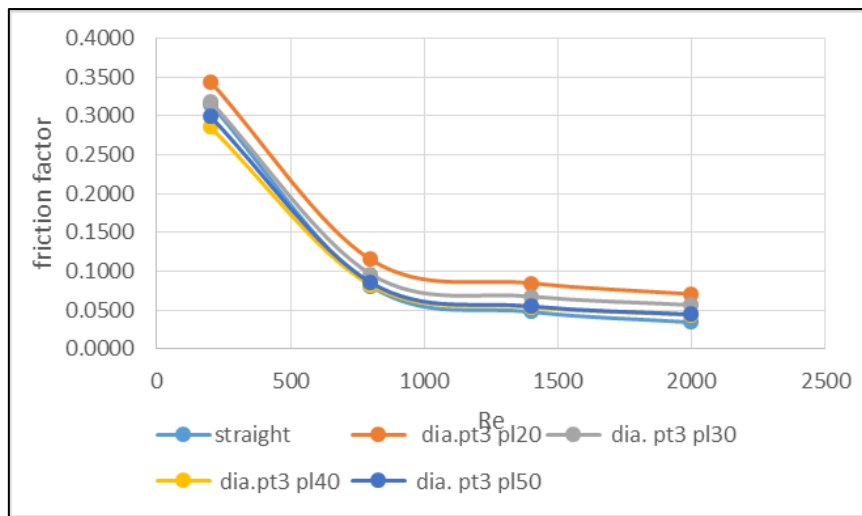


Figure 14: Friction factor versus Reynolds number for different longitudinal pitch lengths for diamond fins inserts

3.3 Velocity Contours

Above all, a first look at the velocity contours in figure 18 may lead to a misunderstanding, in that the velocity values at the walls must be less than that at the core, but in fact, that walls are not walls but symmetries. The velocity contours attached in this study show the flow behavior near the fins regions for different pitch lengths. It is difficult to show the contour for the whole domain because the lateral dimension is very small compared to the longitudinal dimension (2 mm/500 mm). It was found that the contour of each case includes two sections. The first is for the fin area, which is almost identical to all the fins along the channel. The second for the entrance to the channel to show the uniform velocity of the inlet.

It can be seen from the contour that the fluid velocity changes during the length due to the presence of the fins. Therefore, the velocity is as high as possible in the fin area and returns to decrease after the fin. This change works to prevent the flow from reaching the fully developed, so the thermal resistance resulting from the boundary layer of the fluid decreases. This change increases by decreasing the length pitches, as we can see from the velocity values in the contour. We also note that in the area behind the fin where the flow is separated from the wall, the velocity becomes zero. Such a case is an undesirable condition for thermal performance. Also, it can be remarked from the case (1) and (2) that the biconvex fins have a larger stagnant region behind the fins at the same Reynolds number or the separation occurs earlier. The reattachment occurs downstream, and the maximum velocity with biconvex fins in case (2) is less than that of diamond fins in case (1). The increase in transverse pitch length reduces the maximum velocity around the fins. It increases the continuous low-velocity region at the same Reynolds number, such as in cases (4) and (5) of $pt=4$ and $pt=5$ mm, respectively.

Figure 17 shows the local friction factor versus length for a specific pitch length. It shows that the friction factor decreases at the entrance length as in a straight, smooth channel but suddenly increases for all cases and begins to fluctuate at almost fixed values. While for the large pitch length, a fluctuation was noticed because there will be straight sections with lower pressure drop. The velocity core is distorted by the accelerating-decelerating flow and forced to change its directions near the fins. All of this leads to disrupting the boundary layer. It is well known that the pressure drop at the boundary layer growth region or in the developing flow region is very high compared to that in a fully developed region. The fins work to disrupt that

boundary layer, so in a simple term, the boundary layer grows and disrupts periodically, leading to higher pressure drop and higher friction factor.

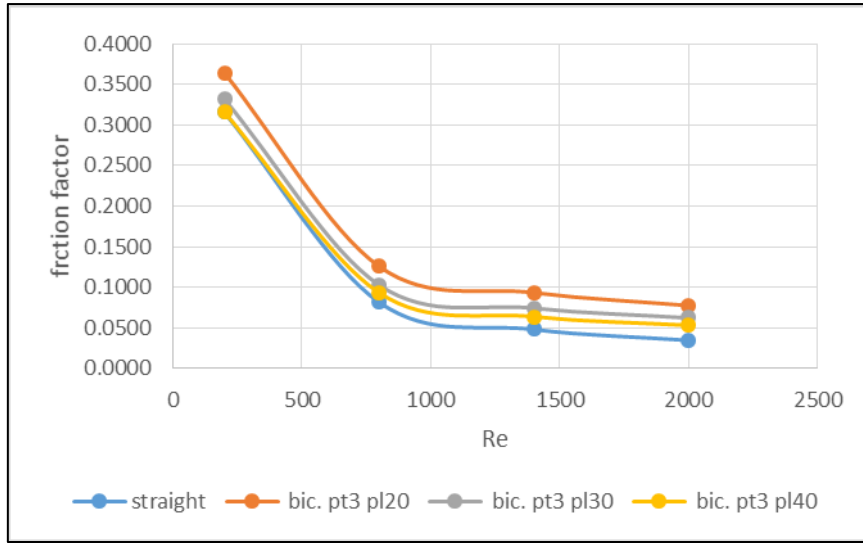


Figure 15: Friction factor versus Reynolds number for different longitudinal pitch lengths for biconvex fins inserts

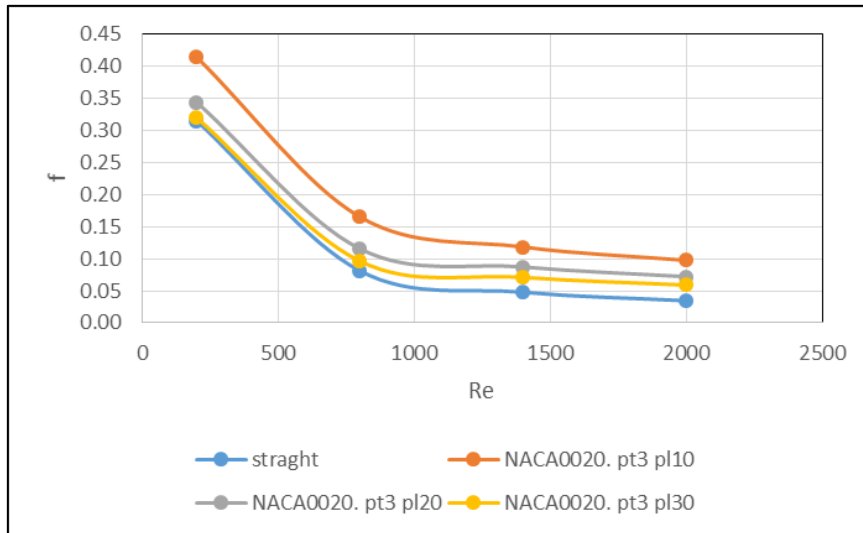


Figure 16: Friction Factor Versus Reynolds Number For Different Longitudinal Pitch Lengths for NACA airfoil fins inserts

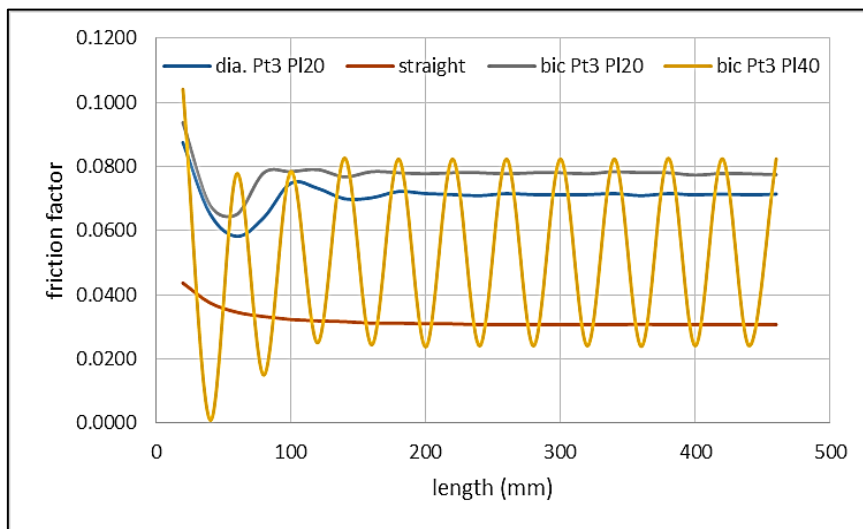


Figure 17: Local friction factor along the channel length

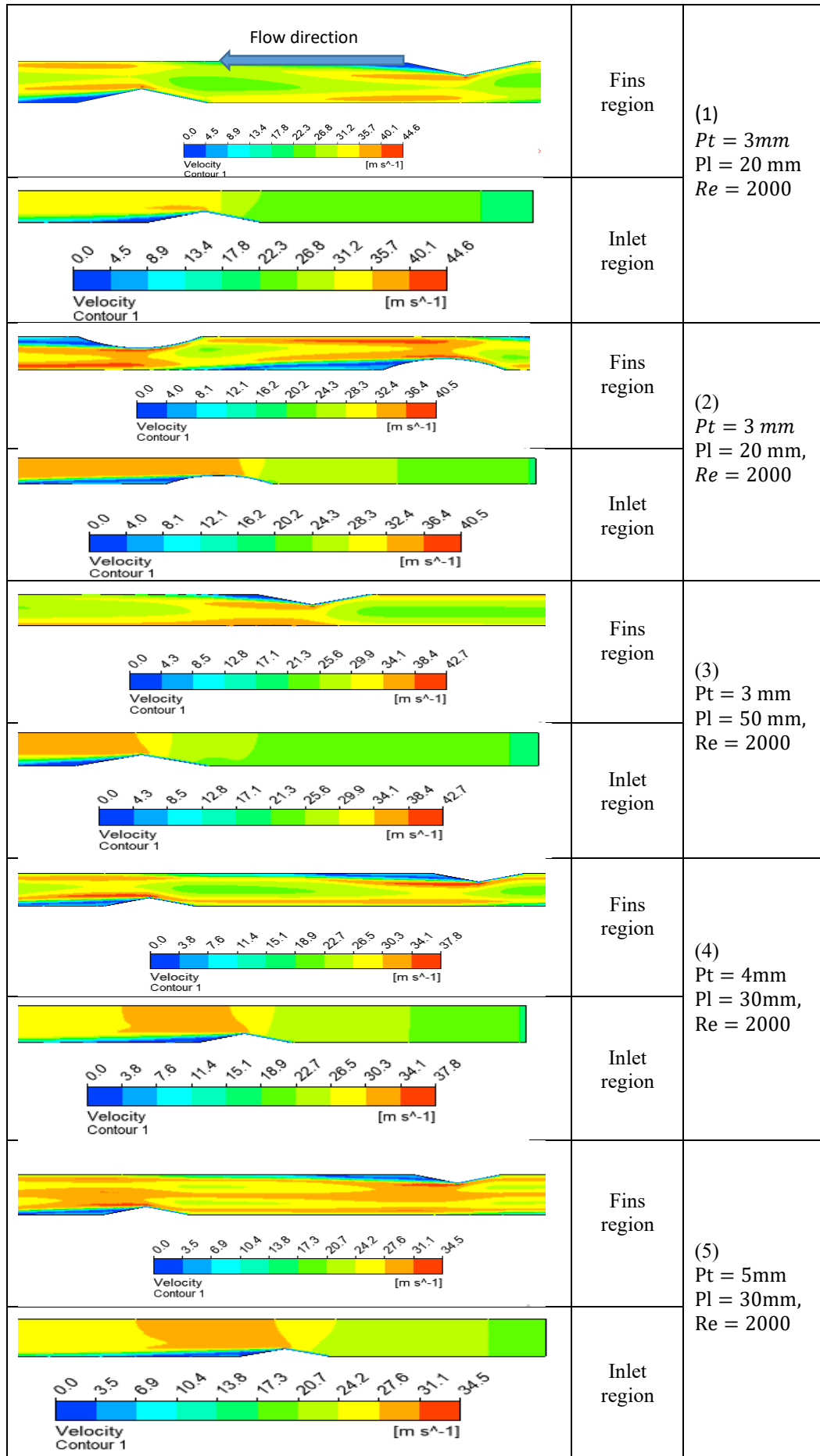


Figure 18: Velocity contour for different C-D channels

3.4 Overall Performance Evaluation Factor (H)

The overall performance evaluation factor can be used for better comparison because it takes account of both thermal performance and pumping power. Figure 19 shows the overall performance of all cases. NACA airfoil fins give the best performance in all Reynolds number ranges. In contrast, the overall enhancement at $pl=20$ mm was up to $\eta=2.75$ because of the high Nusselt number with almost the same friction factor as other fin shapes. On the other hand, the diamond fin gives a moderate performance, while the biconvex fin gives the worst performance.

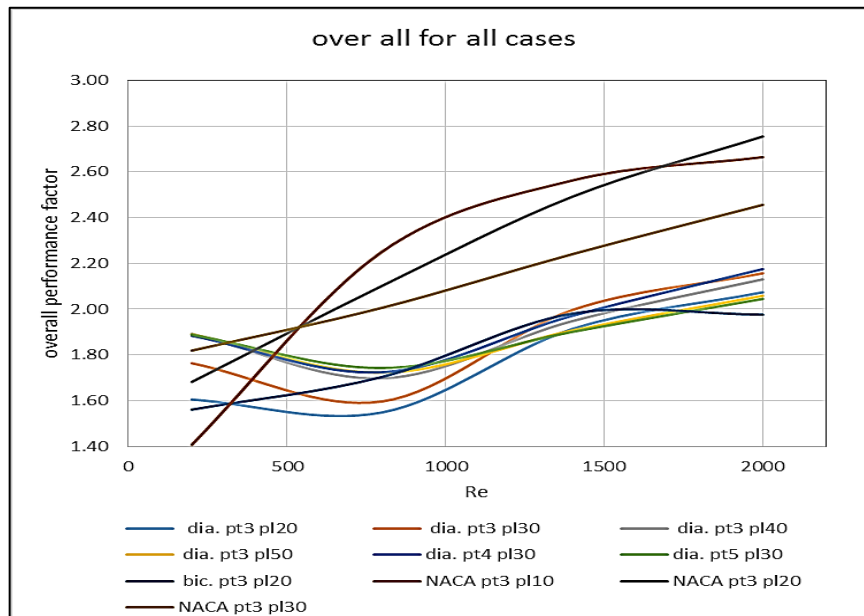


Figure 19: Overall performance evaluation factor Reynolds number for all cases

4. Conclusion

A 3D numerical study was performed to investigate the thermal-hydraulic performance of a PCHE with a new non-uniform channel configuration consisting of three different fins shape inserts: the diamond, biconvex, and NACA0020 airfoil fin shapes. Two geometric parameters were studied, the longitudinal and transverse pitch lengths and three performance parameters were obtained: the Nusselt number, friction factor, and the overall performance evaluation factor. The results show a good enhancement in thermal performance. In comparison, the Nusselt number shows an increase with transverse (pt) and longitudinal (pl) pitch length increment at a low Reynolds number. While, at high Reynolds number, Nusselt number decreases with pt and pl increment. The higher enhancement factor was with NACA airfoil fins at $pt=3$ mm and $pl=20$ mm of $\eta=2.75$ at $Re=2000$, while the worst performance was obtained with biconvex fins. The main reason behind the enhancement is the disruption of the boundary layer and the good mixing induced in the fluid flow.

Acknowledgment

Thanks, must be sent to the department of mechanical engineering at the university of technology, and a lot of thanks sent from a student Ali M. Aljelawy to his teacher Dr. Amer M. Aldabbagh

Author contribution

Methodology Ali M. Aljelawy; Amer M. Aldabbagh; Software and Formal Analysis Ali M. Aljelawy; Amer M. Aldabbagh.; Writing-Original Draft Preparation, Ali M. Aljelawy; Writing-Review & Editing, Ali M. Aljelawy. "All authors have read and agreed to the published version of the manuscript."

Funding

This research received no external funding

Data availability statement

All data underlying the results are available as part of the article, and no additional sources are required.

Conflicts of interest

The authors declare no conflict of interest.

References

- [1] K. Thulukkanam, Heat Exchanger Design Handbook, 2nd Edition, CRC Press, Taylor & Francis Group, 2013.

- [2] A.M. Aneesh, A. Sharma, A. Srivastava, K.N. Vyas, P. Chaudhuri, Thermal-hydraulic characteristics and performance of 3D straight channel based printed circuit heat exchanger, *Appl. Therm. Eng.*, 98 (2016) 474–482. <https://doi.org/10.1016/j.applthermaleng.2015.12.046>
- [3] W. Chu, X. Li, T. Ma, Y. Chen, Q. Wang, Experimental investigation on SCO₂-water heat transfer characteristics in a printed circuit heat exchanger with straight channels, *Int. J. Heat Mass Transf.*, 113 (2017) 184–194. <https://doi.org/10.1016/j.ijheatmasstransfer.2017.05.059>
- [4] S. Lee, K. Kim, S. Kim, Multi-objective optimization of a double-faced type printed circuit heat exchanger, *Appl. Therm. Eng.*, 60 (2013) 44–50. <https://doi.org/10.1016/j.applthermaleng.2013.06.039>
- [5] K. Thulukkanam, *Heat Exchanger Design Handbook*, 2nd Edition, CRC Press, Taylor & Francis Group, 2013.
- [6] A.M. Aneesh, A. Sharma, A. Srivastava, K.N. Vyas, P. Chaudhuri, Thermal-hydraulic characteristics and performance of 3D straight channel based printed circuit heat exchanger, *Appl. Therm. Eng.*, 98 (2016) 474–482. <https://doi.org/10.1016/j.applthermaleng.2015.12.046>
- [7] W. Chu, X. Li, T. Ma, Y. Chen, Q. Wang, Experimental investigation on SCO₂-water heat transfer characteristics in a printed circuit heat exchanger with straight channels, *Int. J. Heat Mass Transf.*, 113 (2017) 184–194. <https://doi.org/10.1016/j.ijheatmasstransfer.2017.05.059>
- [8] S. Lee, K. Kim, S. Kim, Multi-objective optimization of a double-faced type printed circuit heat exchanger, *Appl. Therm. Eng.*, 60 (2013) 44–50. <https://doi.org/10.1016/j.applthermaleng.2013.06.039>
- [9] S. Lee, K. Kim, Thermal Performance of a Double-Faced Printed Circuit Heat Exchanger with Thin Plates, *J. Thermophys. Heat Transf.*, 28 (2014). <https://doi.org/10.2514/1.T4086>
- [10] S.M. Lee, K.Y. Kim, A parametric study of the thermal-hydraulic performance of a zigzag printed circuit heat exchanger, *Heat Transf. Eng.*, 35 (2014) 1192–1200. <https://doi.org/10.1080/01457632.2013.870004>
- [11] S. Baek, J. Kim, S. Jeong, J. Jung, Development of highly effective cryogenic printed circuit heat exchanger (PCHE) with low axial conduction, *Cryogenics*, 52 (2012) 366–374. <https://doi.org/10.1016/j.cryogenics.2012.03.001>
- [12] S. Baik, S. G. Kim, J. Lee, J. I. Lee, Study on CO₂ – water printed circuit heat exchanger performance operating under various CO₂ phases for S-CO₂ power cycle application, *Appl. Therm. Eng.*, 113 (2017) 1536–1546. <https://doi.org/10.1016/j.applthermaleng.2016.11.132>
- [13] I. H. Kim, H. C. No, Thermal hydraulic performance analysis of a printed circuit heat exchanger using a helium-water test loop and numerical simulations, *Appl. Therm. Eng.*, 31 (2011) 4064–4073. <https://doi.org/10.1016/j.applthermaleng.2011.08.012>
- [14] S. G. Kim, Y. Lee, Y. Ahn, J. I. Lee, CFD aided approach to design printed circuit heat exchangers for supercritical CO₂ Brayton cycle application, *Ann. Nucl. Energy*. 92 (2016) 175–185. <https://doi.org/10.1016/j.anucene.2016.01.019>
- [15] S. Lee, K. Kim, Comparative study on performance of a zigzag printed circuit heat exchanger with various channel shapes and configurations, *Heat Mass Transf.*, 49 (2013) 1021–1028. <https://doi.org/10.1007/s00231-013-1149-4>
- [16] S. Lee, K. Kim, Multi-objective optimization of arc-shaped ribs in the channels of a printed circuit heat exchanger, *Int. J. Therm. Sci.*, 94 (2015) 1–8. <https://doi.org/10.1016/j.ijthermalsci.2015.02.006>
- [17] I. Fernández, L. Sedano, Design analysis of a lead – lithium / supercritical CO₂ Printed Circuit Heat Exchanger for primary power recovery, *Fusion Eng. Des.*, 88 (2013) 2427–2430. <https://doi.org/10.1016/j.fusengdes.2013.05.058>
- [18] X. Cui, J. Guo, X. Huai, K. Cheng, H. Zhang, M. Xiang, Numerical study on novel airfoil fins for printed circuit heat exchanger using supercritical CO₂, *Int. J. Heat Mass Transf.*, 121 (2018) 354–366. <https://doi.org/10.1016/j.ijheatmasstransfer.2018.01.015>
- [19] T. L. Ngo, Y. Kato, K. Nikitin, N. Tsuzuki, New printed circuit heat exchanger with S-shaped fins for hot water supplier, *Exp. Therm. Fluid Sci.*, 30 (2006) 811–819. <https://doi.org/10.1016/j.expthermflusci.2006.03.010>
- [20] A. M. Aljelawy, A. M. Aldabbagh, F. F. Hatem, Numerical Investigation of Thermal Hydraulic Performance of Printed Circuit Heat Exchanger of Periodic Diamond Channel Shape, *IOP Conf. Ser. Earth Environ. Sci.*, 961 (2022). <https://doi.org/10.1088/1755-1315/961/1/012010>
- [21] L. M. Jiji, *Heat convection*, 2nd Edition, 2006. <https://doi.org/10.1007/978-3-540-30694-8>
- [22] J.-R. Carlson, Inflow/Outflow Boundary Conditions with Application to FUN3D, *Natl. Aeronaut. Sp. Adm.*, (2011) 1–38.
- [23] M. Chen, X. Sun, R. N. Christensen, I. Skavdahl, V. Utgikar, P. Sabharwall, Pressure drop and heat transfer characteristics of a high-temperature printed circuit heat exchanger, *Appl. Therm. Eng.*, 108 (2016) 1409–1417. <https://doi.org/10.1016/j.applthermaleng.2016.07.149>
- [24] J.E. Hesselgreaves, R. Law, D.A. Reay, *Compact Heat Exchangers Selection, Design and Operation*, Chapter 1 - Introduction, 2nd Edition, Butterworth-Heinemann., (2017) 1–33. <https://doi.org/10.1016/B978-0-08-100305-3.00001-X>